Diatomic molecular-orbital correlation diagrams for Penning and associative ionization*

John C. Bellum and David A. Micha
Quantum Theory Project, Departments of Physics and Chemistry, University of Florida, Gainesville, Florida 32611
(Received 19 May 1976)

The collision processes $A^* + B \rightarrow A + B^+ + e^-$ (Penning ionization) and $A^* + B \rightarrow AB^+ + e^-$ (associative ionization), where A and B are atoms, are considered in terms of the molecular-orbital (MO) correlation diagrams associated with the reactant and product channels. MO correlation diagrams are calculated for $He^*(1s2s) + Ar(3p^6)$ within the multiple-scattering $X\alpha$ one-electron self-consistent-field scheme for both spin-polarized and non-spin-polarized orbitals. The ionization process is discussed in terms of an Auger-type mechanism. By inspecting the MO's involved in the Auger-type process in their united-atoms limit, an analysis is made of the angular momentum contributions needed in describing the emitted electron in the body-fixed frame. A procedure is proposed for constructing MO correlation diagrams based on atomic-orbital energies at the separated- and united-atoms limits, which are determined from readily available data on ground-state energies of neutral atoms. Estimated MO correlation diagrams are presented for the four collision pairs $He^*(1s2s) + Ar(3p^6)$, $+ Kr(4p^6)$, $+ Hg(6s^2)$, and $Ne^*(2p^53s) + Ar(3p^6)$, and in each case an analysis is made of the angular momentum components of the emitted electron in the body-fixed frame. The results confirm that relatively few l values need be included in describing the emitted electron. Our analyses show that it is important to use spin-polarized MO's to obtain detailed behaviors at pseudocrossings, and that the effect of Born-Oppenheimer rotational coupling must be considered, particularly between MO's that converge to the same united-atoms limit.

I. INTRODUCTION

Well known among chemi-ionization processes are Penning and associative ionization (PI and AI) of the type $A^* + B \rightarrow A + B^+ + e^-$ (PI) and $A^* + B \rightarrow AB^+ + e^-$ (AI), where A^* is usually an atom in some metastable state and B is an atom or molecule.[1-5] Experimental information for such collisions includes total ionization cross sections as a function of collision energy,[6-9] angular distributions of heavy particles,[10] and energy distribution[11-13] and angular distribution[14,15] of emitted electrons. Most theoretical effort has been directed at determining the energy dependence of total ionization cross sections and the angular distribution of heavy particles.[16-19] The angular distribution of emitted electrons has been recently studied within a semiempirical model based on molecular-orbital (MO) correlation diagrams.[20] One of our present concerns is to reemphasize the usefulness of MO correlation diagrams as they apply to angular distribution of ejected electrons in PI and AI involving atomic collision partners.

In what follows, we present calculated as well as estimated MO correlation diagrams. Our calculated results are given in Sec. II, where we consider the electronic structure of $He^*(1s2s, {}^{1,3}S) + Ar(3p^6, {}^1S)$ within the multiple-scattering (MS) $X\alpha$ framework.[21,22] We have studied, in the non-spin-polarized approximation, the $K_{Ar}L_{Ar}(\sigma 1s\mathrm{He})^1(\sigma 3s\mathrm{Ar})^2(\sigma 3p\mathrm{Ar})^2(\pi 3p\mathrm{Ar})^4(\sigma 2s\mathrm{He})^1$ configuration of the excited He-Ar diatom whose MO eigenenergies approach the atomic-orbital eigenenergies of $He^*(1s2s)$ and $Ar(3p^6)$ at large internuclear separation, and also the ground $^2\Sigma$ state of the $(He\text{-}Ar)^+$ molecular ion, whose MO eigenenergies approach the atomic levels of $He(1s^2)$ and $Ar^+(3p^5)$ at large internuclear separation. We present some spin-polarized calculations in the neighborhood of a crossing exhibited by our non-spin-polarized calculations, and comment on the conditions under which the noncrossing rule applies for MO eigenenergies.

Keeping in mind our calculated results, in Sec. III we consider PI and AI processes in terms of MO correlation diagrams. Analyzing the ionization on the basis of an Auger-type process, we can identify MO's which, together with the continuum state of the emitted electron, are involved in the process. Inspecting the united-atoms limit. in the center-of-mass, body-fixed frame then permits a determination of the angular momenta which contribute to the continuum state of the emitted electron.

In Sec. IV we describe a procedure for estimating MO correlation diagrams which makes use of available data on atomic-orbital energies, and of two basic guidelines. Application is made there to the pairs $He^*(1s2s)+Ar(3p^6)$, $+Kr(4p^6)$, $+Hg(6s^2)$, and $Ne^*(2p^53s)+Ar(3p^6)$. The resulting estimated MO correlations for these systems are then analyzed according to Sec. III to determine the minimal set of angular momentum l values which are needed in each case to describe emitted electrons

in the body-fixed frame. Finally, in Sec. V we discuss the results of this work and their significance.

II. MO CALCULATIONS FOR He*+Ar AND He+Ar$^+$

An adequate understanding of atomic and molecular collision phenomena requires information on electronic structure as a function of the changing internuclear separations. Such information is needed in order to describe inelastic processes involving electronic excitation and charge transfer as well as ionization. In this regard we have earlier pointed out the usefulness of one-electron MO approaches in describing electronic structure, in that such approaches afford a self-consistent calculational framework of minimal complexity which can treat ground as well as excited electronic states.[23] Chemi-ionization is a prime example of a process where electronically excited states play a crucial role. We have considered as a representative case Penning and associative ionization in $He^*(1s2s, {}^{1,3}S) + Ar(3p^6, {}^1S)$ collisions. Here, calculations are needed for the excited states of the He-Ar diatom which separate appropriately to $He^*(1s2s, {}^{1,3}S)$ and $Ar(3p^6, {}^1S)$, and for the states of $(He\text{-}Ar)^*$ which separate to $He(1s^2, {}^1S)$ and $Ar^+(3p^5, {}^2P)$.

Following our previous work, we have performed calculations within the MS $X\alpha$ one-electron MO framework,[21,22] which uses the $X\alpha$ statistical approximation to electronic exchange and the conventional MS computational scheme. We mention here only some of the essential features of the $X\alpha$ theory. The total energy $E_{X\alpha}$ of a system of N electrons is an energy functional of a set of spin orbitals, $\{\phi_i\}$, and their occupation numbers $\{n_i\}$, and, accordingly, we identify an electronic state at internuclear separation R as being associated with a given assignment of the n_i. Variation of $E_{X\alpha}$ with respect to the ϕ_i requires that the ϕ_i of a given spin satisfy a set of one-electron eigenvalue equations which can be written

$$h^{\uparrow}_{\text{eff}}(\vec{r}_1)\phi_i(\vec{r}_1) = \epsilon_i \phi_i(\vec{r}_1). \tag{1}$$

$h^{\uparrow}_{\text{eff}}(\vec{r}_1)$ is the effective one-electron Hamiltonian for electrons of spin up, and, using our previous notation,[23]

$$h^{\uparrow}_{\text{eff}}(\vec{r}_1) = f_1(\vec{r}_1) + \int d\vec{r}_2 \frac{2\rho(\vec{r}_2)}{r_{12}} - 6\alpha[(3/4\pi)\rho^{\uparrow}(\vec{r}_1)]^{1/3}, \tag{2}$$

where

$$f_1(\vec{r}_1) = -\nabla_1^2 + \sum_{\alpha} \frac{-2Z_\alpha}{r_{1\alpha}};$$

$$\rho(\vec{r}) = \rho^{\uparrow}(\vec{r}) + \rho^{\downarrow}(\vec{r}) = \sum_{i^{\uparrow}} n_i \phi_i^*(\vec{r})\phi_i(\vec{r}) + \sum_{i^{\downarrow}} n_i \phi_i^*(\vec{r})\phi_i(\vec{r}) \tag{3}$$

is the charge density comprised of the contributions from electrons of spin up and spin down. In the non-spin-polarized (NSP) approximation,

$$\rho^{\uparrow}(\vec{r}) = \rho^{\downarrow}(\vec{r}) = \tfrac{1}{2}\rho(\vec{r}),$$

which means that the orbitals of spin up and spin down become identical, and each orbital can be considered as accommodating as many electrons of spin up as of spin down.

In our calculations we have proceeded first with a NSP treatment. According to the multiple-scattering computational scheme, each self-consistent calculation begins with a potential which is the "muffin-tin" form of a superposition of atomic potentials centered at each atomic site of the molecule. Therefore for the He-Ar excited state we used $Ar(3p^6)$ and NSP $He^*(1s2s)$ Hartree-Fock-Slater (HFS) potentials,[24] and for the He-Ar ionic state we used $He(1s^2)$ and NSP $Ar(3p^5)$ HFS potentials. For both the excited molecule and the molecular ion, the electronic states were specified by occupying the MO's so that their eigenenergies were correctly separating at large internuclear separations to the corresponding atomic-orbital eigenenergies of the above-mentioned HFS atomic calculations. In other words, we let the boundary conditions of the PI and AI processes at large R determine the appropriate excited and ionic states of the He-Ar molecule. Heteronuclear molecules require a choice for the radii of the spherical regions centered at each atomic site. In our earlier treatment of the ground-state He-Ar molecule[23] we took the ratio of the He to the Ar sphere radii to be $\langle r_{1s}\rangle_{\text{He}}/\langle r_{3p}\rangle_{\text{Ar}} \simeq 0.927\,27/1.662\,96 \simeq 0.5576$, where, e.g., $\langle r_{1s}\rangle_{\text{He}}$ denotes the average value of r for the $1s$ orbital of $He(1s^2)$. The situation for $(He\text{-}Ar)^+$ is roughly the same as for He-Ar, since we calculate $\langle r_{3p}\rangle$ for $Ar^+(3p^5)$ (NSP) to be $1.549a_0$. Thus for the molecular ion we used the ratio of 0.5576 at all R. On the other hand, $He^*(1s2s)+Ar(3p^6)$ is quite another case, since the $2s$ orbital of $He^*(1s2s)$ is very diffuse. Our NSP results show $\langle r_{2s}\rangle$ of $He^*(1s2s)$ to be about $4.546a_0$. Because of this diffuseness, we decided to choose the ratio of the He to the Ar sphere radii by finding which of its values minimized the total energy of the specified excited state of He-Ar at a fairly large R, namely, $R = 9.0a_0$. In this way, a ratio of 1.4 was found, which we used then at all R for the excited state of He-Ar. The values of the factor α in the various muffin-tin regions of the molecule, for both the excited as well as ionic states, were those used previously in the ground-state He-Ar calculations, and the specific computational details also remain as reported earlier.[23]

The results of our NSP MS $X\alpha$ calculations are displayed in Figs. 1 and 2, respectively, for the

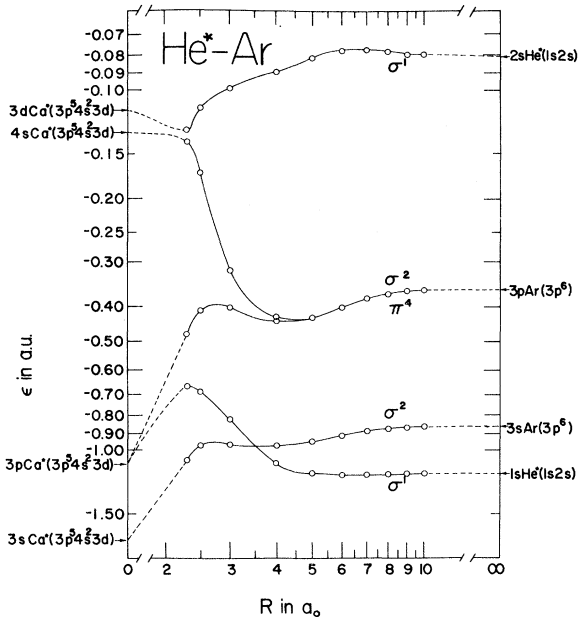

FIG. 1. MO correlation diagram from NSP MS $X\alpha$ calculations of the He-Ar diatom in the excited Σ configuration which separates at large R to $He^*(1s2s) + Ar(3p^6)$. Calculated points are circled.

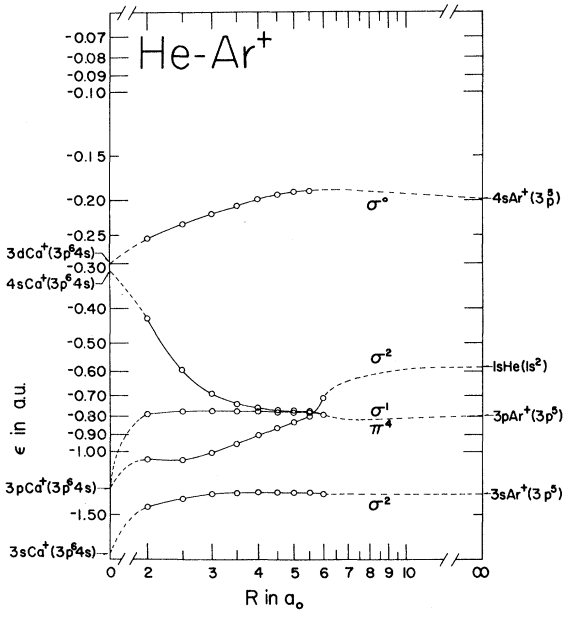

FIG. 2. MO correlation diagram from NSP MS $X\alpha$ calculations of the $(He\text{-}Ar)^+$ molecular ion in the ground Σ state which separates at large R to $He(1s^2) + Ar^+(3p^5)$. Calculated points are circled.

excited state of the He-Ar diatom and the ground state of the He-Ar molecular ion which are appropriate to PI and AI. Shown on log-log plots are the MO eigenenergies versus R for $2.3a_0 \leq R \leq 10.0a_0$ in the case of the excited molecule and $2.0a_0 \leq R \leq 6.0a_0$ in the case of the molecular ion. The MO eigenenergies are labeled according to their symmetry and occupation number. In each case, the NSP HFS atomic-orbital eigenenergies for the separated atoms are shown at the right-hand side of the plot, and the dashed lines indicate how each MO eigenenergy is properly approaching its respective separated-atoms (SA) limit. In the united-atoms (UA) limit we expect the excited He-Ar molecule to approach $Ca^*(3p^5 4s^2 3d)$ and the ground-state molecular ion to approach $Ca^+(3p^6 4s)$. The atomic-orbital eigenenergies from NSP HFS calculations on these united atoms are appropriately shown at the left-hand side of each plot, and while the MO eigenenergies may exhibit much structure between the region of $2a_0$ and the UA limit, the dashed lines at the left-hand side of each plot show that these UA limits are not unreasonable. In both plots, the label for the σ MO arising at large R from $3p$ Ar appears above the π MO label. In fact, this ordering for those levels is valid only for $R \lesssim 5a_0$. For $R \gtrsim 6a_0$, the π level lies above the σ level, but they are too close together at large R to be distinguishable on our plot.

In Fig. 1 we show a crossing near $3.5a$ occurring between the doubly and singly occupied NSP σ orbitals arising, respectively, at large R from $3s$ $Ar(3p^6)$ and NSP $1s$ $He^*(1s2s)$. This crossing would appear to violate the noncrossing rule for the MO eigenenergies, and warrants a detailed analysis. The orbitals of a given symmetry are ordered according to their eigenenergies, obtained self-consistently from Eq. (1). This equation is an eigenvalue equation involving an effective Hamiltonian determined at each R according to Eq. (2). To establish the noncrossing rule for the eigenenergies of Eq. (1), one expresses the effective Hamiltonian at a supposed crossing R_c in terms of its expansion about $R = R_c + \delta R$ located a small distance δR from R_c:

$$h^{\uparrow}_{\text{eff}}(R_c) = h^{\uparrow}_{\text{eff}}(R) - (dh^{\uparrow}_{\text{eff}}/dR)_{R_c}\delta R .$$

The noncrossing rule follows by noting that $(dh^{\uparrow}_{\text{eff}}/dR)_{R_c}\delta R$ is a perturbation which lifts any degeneracy in the eigenvalue spectrum at R_c. However, if $h^{\uparrow}_{\text{eff}}(R)$ is made to be discontinuous by choice, the conditions of the noncrossing rule no longer apply.

Referring to Eq. (2), the R dependence of the effective Hamiltonian appears explicitly in $f_1(\vec{r}_1)$ and implicitly in the charge density ρ. Showing the full R dependence, we may then write the effective Hamiltonian as $h^{\uparrow}_{\text{eff}}(\vec{r}_1; R, \rho(\vec{r}_1, R))$, and

$$\frac{dh^{\dagger}_{\text{eff}}}{dR} = \frac{\partial h^{\dagger}_{\text{eff}}}{\partial R}\bigg|_{\rho} + \frac{\delta h^{\dagger}_{\text{eff}}}{\delta \rho}\frac{d\rho}{dR}. \tag{4}$$

The term $d\rho/dR$ in Eq. (4) can be seen, from Eq. (3), to involve derivatives of the orbitals and occupation numbers with respect to R. As long as the n_i and ϕ_i are continuous in their R dependence, $dh^{\dagger}_{\text{eff}}/dR$ will be well behaved, and the noncrossing rule will hold. However, if the occupation numbers are changed discontinuously in some region of R, then the noncrossing rule will no longer be valid in that region. These considerations apply as well to the NSP effective Hamiltonian, and in fact, in our case, as shown in Fig. 1, a discontinuous change in occupation numbers does occur. To the right-hand side of the crossing, the σ orbitals, in order of increasing eigenenergy, have occupation numbers 1, 2, 2, and 1. To the left-hand side of the crossing, they are 2, 1, 2, and 1. We investigated further the region of the crossing by doing spin-polarized calculations at $R = 3.0a_0$, $3.5a_0$, and $4.0a_0$ in the case of the $^3\Sigma$ excited state which separates at large R to $\text{Ar}(3p^6, {}^1S)$ and $\text{He}^*(1s2s, {}^3S)$. In Fig. 3 we restrict our attention to the levels of the NSP σ^2 and σ^1 MO's which cross in Fig. 1, and contrast them with their spin-split counterparts calculated in the region $3.0a_0 \leq R \leq 4.0a_0$ as well as at the UA and SA limits.

It is important to note that for $R \gtrsim 3.5a_0$ the NSP σ^1 orbital of He* is split considerably into its occupied component of spin-up σ^1_α and its unoccupied component of spin-down σ^0_β, on out to the SA limit, where the splitting is between the unoccupied $1s_\beta$ and the occupied $1s_\alpha$ of $\text{He}^*(1s2s, {}^3S)$. The σ^2 orbital from Ar is split only slightly into each of its occupied spin components. Crossings between two orbital eigenenergies of different spin components are permitted, since each involves a different effective Hamiltonian [see Eq. (2)]. Between $3.5a_0$ and $4.0a_0$ we find such a crossing for the two spin components that split from the NSP σ^2 orbital of Ar, and in fact, as R decreases, the σ^1_β level from $3s_\beta$ $\text{Ar}(3p^6, {}^1S)$ is decreasing in energy to pair up with the occupied σ^1_α level from $1s_\alpha$ $\text{He}^*(1s2s, {}^3S)$, whereas its spin-up partner from $3s_\alpha$ $\text{Ar}(3p^6, {}^1S)$ is rising to pair up with the (empty) σ^0_β level from $1s_\beta$ $\text{He}^*(1s2s, {}^3S)$. In the UA limit, this empty σ^0_β level will correlate with the partially occupied $3p_\beta$ atomic orbital of $\text{Ca}^*(3p^5 4s^2 3d, {}^3L)$.

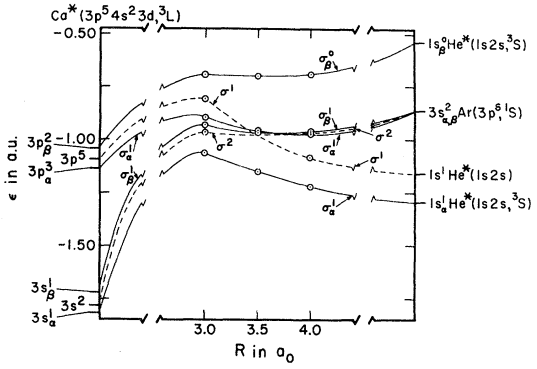

FIG. 3. Spin-polarized (solid lines) MO eigenenergies calculated for the excited $^3\Sigma$ configuration of the He-Ar diatom which separates at large R to $\text{He}^*(1s2s, {}^3S) + \text{Ar}(3p^6, {}^1S)$, and their NSP counterparts (dashed lines) from Fig. 1. The eigenenergies are those arising at large R from the 1s He* and 3s Ar atomic orbitals, and are shown in the neighborhood of the crossing near $3.5a_0$ in Fig. 1. Those associated with spin-polarized orbitals are labeled according to their spin (α or β). Calculated points are circled.

Such a spin-polarized analysis as this confirms the choice of occupation numbers of our NSP calculations for which the vacancy associated with the NSP σ^1 orbital is correlating in the UA limit with the partially occupied $3p$ atomic orbital of $\text{Ca}^*(3p^5 4s^2 3d)$. This feature will prove important in our considerations later on regarding the angular momentum contributions to the continuum state of the electron emitted during PI and AI. The crossing shown in Fig. 2, between the NSP singly and doubly occupied σ orbitals of the molecular ion near $5.5a_0$, is another example of a discontinuous change in occupation numbers, which in this case is required to reach the appropriate SA limit.

III. ANALYSIS OF PI AND AI PROCESSES BASED ON MO CORRELATION DIAGRAMS

We now consider how an MO correlation-diagram study, such as we have described in Sec. II, can help in understanding what takes place in PI and AI processes. Collisional ionization occurs for R greater than the distance of closest approach, which in the case of He*+Ar is around $7a_0$ at thermal collision energies. Referring to our calculated MO diagram in Fig. 1, we observe that in this range of R there is a vacancy associated with the σ^1 MO arising from 1s He* at large R, above which are some fully occupied MO's as well as the singly occupied σ^1 MO arising from 2s He* at large R. This situation suggests that the ionization may proceed by an Auger-type process. Namely, two electrons in higher-lying orbitals participate in ionization as one of them is promoted to a continuum state while the other drops to fill the vacancy associated with the σ^1 MO arising from SA 1s He*. We may characterize the process as one in which initially the two electrons are in MO's ϕ_1 and ϕ_2, while finally

(after ionization) they are in MO's ϕ_1' and ϕ_2', where ϕ_1' designates the continuum state of the ionized electron, having momentum k and angular momentum components l_1'.

If the wave function $\psi_a(N)$ is associated with the system of N electrons before ionization, and $\psi_b(k,N-1)$ is associated with the system of $N-1$ electrons plus the emitted electron in its continuum state after ionization, then, in the body-fixed (BF) frame, the transition probability for ionization involving these two wave functions is expressed in terms of the interaction matrix element, $V_{ba}(R,k)_{\mathrm{BF}}$, where

$$V_{ba}(R,k)_{\mathrm{BF}}=\langle\psi_b(k,N-1)|H_{\mathrm{el}}-E|\psi_a(N)\rangle_{\mathrm{BF}}. \quad (5)$$

Here H_{el} is the electronic Hamiltonian for the N electrons, E is the total energy, and the brackets indicate integration over electronic variables. Within a single-determinant description, ψ_b will differ from ψ_a in that the one-electron orbitals ϕ_1 and ϕ_2 of ψ_a are replaced by ϕ_1' and ϕ_2' to obtain ψ_b. As a consequence Eq. (5) reduces to a sum of direct and exchange contributions, which we write, respectively, as

$$\begin{aligned} V_D(R,k)&=\langle\phi_1'\phi_2'|v|\phi_1\phi_2\rangle_{\mathrm{BF}},\\ V_E(R,k)&=\langle\phi_1'\phi_2'|v|\phi_2\phi_1\rangle_{\mathrm{BF}}, \end{aligned} \quad (6)$$

where $v=1/r_{12}$, the electron-electron Coulomb interaction in atomic units.

In Fig. 4(a) we show a schematic MO correlation diagram for the He*$(1s2s)$+Ar$(3p^6)$ case. The construction of such estimated MO correlation diagrams will be discussed in Sec. IV. The MO energies at large R represent levels at the time of ionization. For instance, referring to Fig. 4(a), two electrons, one initially in $\sigma 2s$ from He* and the other in $\pi 3p$ from Ar, could participate in an Auger process whereby one is promoted to a continuum state while the other fills the $\sigma 1s$ vacancy from He*. That is, $\phi_1=\sigma 2s$, $\phi_2=\pi 3p$, the continuum state $\phi_1'=(k,l_1',m_1')$, and $\phi_2'=\sigma 1s$.

MO correlation diagrams, such as that shown in Fig. 4(a), allow us to predict the minimal number of angular momentum contributions l_1' which are necessary to describe the continuum state of the emitted electron in the BF frame. We proceed by following the MO's involved in ionization towards their UA limit. With the exception of the continuum state ϕ_1', MO's correlate in the UA limit to atomic orbitals of well-defined angular momentum. That is, we can write

$$\begin{aligned} &\phi_1\xrightarrow{\mathrm{UA}}\chi_1(l_1,m_1),\quad \phi_2\xrightarrow{\mathrm{UA}}\chi_2(l_2,m_2),\\ &\phi_1'\xrightarrow{\mathrm{UA}}\chi_1'(k,l_1',m_1')\ \text{(continuum)},\quad \phi_2'\xrightarrow{\mathrm{UA}}\chi_2'(l_2',m_2'), \end{aligned} \quad (7)$$

where the χ's refer to the UA (atomic) orbitals.

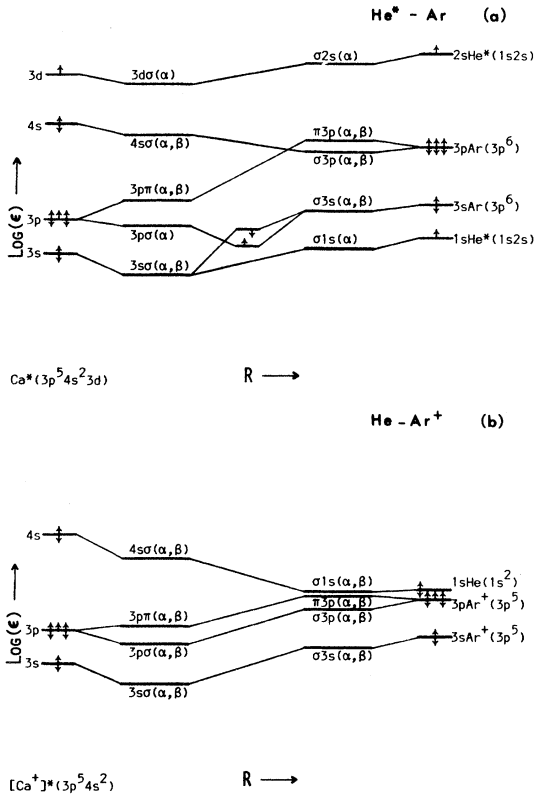

FIG. 4. Estimated MO correlation diagrams for (a) He*$(1s2s)$+Ar$(3p^6)$ and (b) He$(1s^2)$+Ar$^+(3p^5)$.

Looking also at the direct and exchange matrix elements in the UA limit, Eq. (6) becomes

$$\begin{aligned} V_D(R,k)&\xrightarrow{\mathrm{UA}}V_D^{\mathrm{UA}}(k)=\langle\chi_1'\chi_2'|v|\chi_1\chi_2\rangle_{\mathrm{BF}},\\ V_E(R,k)&\xrightarrow{\mathrm{UA}}V_E^{\mathrm{UA}}(k)=\langle\chi_1'\chi_2'|v|\chi_2\chi_1\rangle_{\mathrm{BF}}. \end{aligned} \quad (8)$$

Next, using the notation of previous work,[25] we express the electron-electron Coulomb interaction as an expansion in terms of its multipole components,

$$\frac{1}{r_{12}}=\frac{1}{r_>}\sum_{L=0}^{\infty}\left(\frac{r_<}{r_>}\right)^L P_L(\cos\theta_{12}), \quad (9)$$

and write Eq. (8) as follows:

$$\begin{aligned} V_D^{\mathrm{UA}}(k)&=\delta(s_1',s_1)\delta(s_2',s_2)\\ &\quad\times\sum_{L=0}^{\infty}F_L(1'2'12)A_L(1'2'12),\\ V_E^{\mathrm{UA}}(k)&=\delta(s_1',s_2)\delta(s_2',s_1)\\ &\quad\times\sum_{L=0}^{\infty}F_L(1'2'21)A_L(1'2'21). \end{aligned} \quad (10)$$

The factors F_L and A_L are proportional to products

of 3-j coefficients,

$$F_L(1'2'12)=\frac{[(2l_1'+1)(2l_2'+1)(2l_1+1)(2l_2+1)]^{1/2}}{2L+1}\times\begin{pmatrix} l_1' & L & l_1\\ 0 & 0 & 0\end{pmatrix}\begin{pmatrix} l_2' & L & l_2\\ 0 & 0 & 0\end{pmatrix}R_L(1'2'12), \tag{11}$$

$$A_L(1'2'12)=(-1)^{m_1'+m_2'+M}(2L+1)\times\begin{pmatrix} l_1' & L & l_1\\ -m_1' & -M & m_1\end{pmatrix}\begin{pmatrix} l_2' & L & l_2\\ -m_2' & M & m_2\end{pmatrix}.$$

The $R_L(1'2'12)$ are Coulomb integrals involving the radial parts of the orbitals in the UA limit, and depend on their principal as well as angular momentum quantum numbers. The presence of the 3-j coefficients in the F_L and A_L factors of Eq. (11) reflects the coupling of the angular momenta of the electrons due to the 2^L multipole component of the electron-electron Coulomb interaction and allows us to specify the ranges of values of l_1' and m_1' for which contributions will appear in the direct and exchange matrix elements of Eq. (10). This is accomplished by employing the selection rules for the 3-j coefficients.[26] In the UA limit, (l_1m_1), (l_2m_2), and $(l_2'm_2')$ are known. Therefore, referring to Eq. (11), one of the 3-j factors in F_L specifies the allowed range of L, and similarly one of the 3-j factors in A_L further specifies the range of M. Once the ranges of L and M have been determined, the remaining 3-j coefficient factors, one in F_L and one in A_L, specify the ranges of l_1' and m_1' for the continuum state of the emitted electron.

Thus for the direct matrix element of Eq. (10) we find L and M restricted as follows:

$$|l_2'-l_2|\le L\le l_2'+l_2,\qquad (l_2'+l_2+L)\ \text{even},\quad -m_2'+M=-m_2. \tag{12}$$

For each L and M possible from Eq. (12), the remaining two factors in F_L and A_L restrict l_1' and m_1' in similar fashion:

$$|l_1-L|\le l_1'\le l_1+L,\qquad (l_1+L+l_1')\ \text{even},\quad m_1'+M=m_1. \tag{13}$$

Interchanging the indices 1 and 2 among the primed symbols in Eqs. (12) and (13) provides corresponding expressions for the exchange matrix element of Eq. (10).

Thus far our discussion has been only in terms of the interaction matrix element of Eq. (5) between two determinantal wave functions ψ_a and ψ_b distinguished from one another, respectively, by the MO's ϕ_1 and ϕ_2 before ionization and ϕ_1' and ϕ_2' after ionization.

We now consider the manifold of determinantal states ψ_a which is needed to represent the electronic state ψ_i before ionization. Each of those states ψ_a has an angular momentum component along the molecular axis, Λ_a, equal to the absolute value of the sum of axial angular momentum components of the MO's from which the determinantal wave function is constructed. To the extent that one may neglect rotational Born-Oppenheimer couplings, only determinants ψ_a having $\Lambda_a=\Lambda_i$ are needed in representing the state of the electrons prior to ionization, where Λ_i denotes the axial component of electronic angular momentum in the SA limit of the incident channel. However, Born-Oppenheimer couplings cannot be neglected in the UA limit because of their R^{-2} dependence.[27,28] Hence in order to properly carry out the UA analysis just described we must include contributions from states ψ_a for which $\Lambda_a-\Lambda_i=0,\pm1$.

For example, according to the MO correlation diagram of Fig. 4(a), one constructs the leading determinantal wave function prior to ionization from the MO's, shown at the right-hand side, which correlate to the occupied SA atomic orbitals, and one observes that $\Lambda_i=0$. We had mentioned earlier the possible case of an Auger-type process in which we identified the participating orbitals ϕ_1 and ϕ_2 with $\sigma 2s$ He* and $\pi 3p$ Ar, respectively. Not shown in Fig. 4(a) are levels of MO's associated with unoccupied SA atomic orbitals. Among these MO's there may be one whose axial component of angular momentum differs by ±1 from that of an occupied MO with which it shares the same UA atomic-orbital limit. An example of such a case is the $\pi 2p$ MO arising from the unoccupied SA $2p$ orbital of He*$(1s2s)$ and the $\sigma 2s$ MO of Fig. 4(a), both of which correlate in the UA limit to the singly occupied $3d$ atomic orbital of Ca*$(3p^54s^23d)$. Replacing the $\sigma 2s$ MO of the previously described Σ determinant by this $\pi 2p$ MO would result in a Π determinant which is significant for our UA analysis, due to Born-Oppenheimer couplings. In the Σ case ϕ_1 of the Auger-type process would be identified by $\sigma 2s$, in the Π case with $\pi 2p$. According to Eq. (7), the UA limit results in $l_1=2$, $m_1=0$ for the Σ case and $l_1=2$, $m_1=\pm1$ for the Π case. This means that in applying Eqs. (12) and (13) for these two cases, the restrictions on the l values are the same for both, while the m-value restrictions involve $m_1=0$ for Σ and $m_1=\pm1$ for Π determinants.

In general, then, our UA analysis of the angular momentum contributions to the emitted electron requires that we write the initial electronic state prior to ionization as a linear combination of such

determinants,

$$\psi_i = \sum_a \psi_a C_a .$$

Similar considerations hold after ionization, where a manifold of determinants ψ_b results, each differing from the other by the particular continuum state ϕ_1' associated with it. The final electronic state then is written

$$\psi_f = \sum_b \psi_b C_b ,$$

and the total transition probability for ionization is expressed in terms of $V_{fi}(R,k)_{\mathrm{BF}}$, which is a linear combination of interaction matrix elements of Eq. (5),

$$V_{fi}(R,k)_{\mathrm{BF}} = \sum_{a,b} C_b^* C_a V_{ba}(R,k)_{\mathrm{BF}} .$$

According to this general description, we may apply Eqs. (12) and (13) of our UA analysis using the l-value restrictions directly with values found from a MO correlation diagram such as in Fig. 4(a), but remembering that the m-value restrictions are weakened due to Born-Oppenheimer couplings.

Of course, ionization occurs far from the UA limit, and the values for l_1' which we obtain are certainly not all those which should be included, but they do constitute the minimal set required for making a reasonable physical description of the emitted electron. That such a minimal set can be specified is important for the parametrization of expressions at various levels of approximation by which calculations of angular distributions of the emitted electrons can be made.[15,20]

IV. ESTIMATING MO CORRELATION DIAGRAMS FOR DIATOMICS

An analysis such as we have just outlined requires only schematic correlation diagrams which should, however, be reliable in relating SA and UA limits of the higher-lying MO's. In this section we will describe a procedure for estimating MO correlation diagrams, and apply it to the collision pairs $He^*(1s2s) + Ar(3p^6)$, $+Kr(4p^6)$, $+Hg(6s^2)$, and $Ne^*(2p^5 3s) + Ar(3p^6)$. Based on these estimated MO correlation diagrams and the analysis of Sec. III, we will then determine the minimal set of angular momentum contributions required to describe the emitted electrons in PI and AI.

In order to begin constructing estimated MO correlation diagrams, one must have the appropriate SA and UA atomic-orbital energy levels of the collision partners both before and after ionization. We have found the following scheme to be sufficiently reliable and simple to apply. For the ground-state levels of neutral atoms we use any of the results of Hartree-Fock or Hartree-Fock-Slater calculations, which are available in tabulated form in the literature.[29-32] Furthermore, we rely on these calculated atomic-orbital energy levels for ground-state neutral atoms in order to obtain the levels of the ground- and excited-state atomic ions and of excited-state neutral atoms. Clementi and Roetti have published results of Hartree-Fock calculations on ground states of atomic ions as well as neutral atoms for $Z \leq 54$.[32] Comparison of these results shows that the spacing between the levels of any two of the higher occupied orbitals of the neutral atoms is very nearly preserved for the corresponding two orbitals of the atomic ions. This observed property of the Hartree-Fock orbitals lends itself well to a quite accurate determination of the levels of ground-state ions for all of the atoms. We simply locate the level of the highest occupied orbital at the ionization potential of the atomic ion in question,[33] below which the next few levels are positioned according to their relative spacing in the corresponding neutral atom.

The levels of excited states of neutral atoms and atomic ions involve somewhat more uncertainty in their determination. The essential requirement these levels should satisfy is that of being properly ordered with respect to energy. Within an atomic-orbital framework, basically two types of excited states may occur. First are the excited states formed from the ground state by promotion of an electron(s) from an inner shell to a higher level previously completely unoccupied in the ground state [such as $Ca(3p^6 4s^2) \rightarrow Ca^*(3p^5 4s^2 3d)$]. Second are the excited states formed from the ground state by promotion of an electron(s) from an inner shell to a higher level previously partially occupied in the ground state [such as $Pb(5d^{10}6s^2 6p^2) \rightarrow Pb^*(5d^9 6s^2 6p^3)$]. In this second case, the excited state involves only altering the occupation numbers of orbitals already partially occupied in the ground state, and, although levels will be shifting due to this, we expect that the levels of the excited state will be well described by those of the parent ground state. However, in the first case mentioned above, we treat the promoted electron(s) as moving in the field of the remaining electrons in the ionic state characterized by the appropriate vacancy(s). We therefore determine the ionic core levels as we have already described, and then apply a version of Slater's rules,[34] based on estimated screening factors, to describe the level(s) of the promoted electron(s) in the presence of the ionic core.

We now turn to the construction of the schematic MO correlation diagrams. In order to proceed, we rely on the following fundamental guidelines: (a) We consider only those MO levels which conform at the SA limit to given atomic-orbital levels of either the reactant or product collision partners. (b) The MO levels, for both the excited molecule and the molecular ion, correlate from SA to UA limits in accordance with the noncrossing rule for spin-polarized orbitals. The specific example of $He^*(1s2s)+Ar(3p^6)$ will show how we apply these guidelines. Referring to Fig. 4(a), on the right-hand side are displayed the occupied levels of $He^*(1s2s)$ and $Ar(3p^6)$, determined as described above. We point out that our procedure for estimating levels of excited atoms leaves some uncertainty as to effects of spin splittings. Normally, except for the high-lying level of the promoted electron in an excited atom, we expect splitting due to spin polarization to be small compared to the relative spacings of the levels. However, helium in its $1s2s$ excited states is a rather special case, since there are only two electrons. The estimates we make of the occupied $1s$ and $2s$ levels of excited helium (based on estimated screening factors) are certainly reasonable, especially in relation to the $3s$ and $3p$ levels of $Ar(3p^6)$. But each of these occupied levels has associated with it the level of its unoccupied partner of opposite spin. The unoccupied $1s$ level of He^* may lie below or above the $3s$ level of $Ar(3p^6)$, depending on whether there is a weak or a strong splitting of the two $1s$ spin components (one occupied and one unoccupied). Applying our guidelines (a) and (b) to the case of weak splitting, we would find the SA levels correlating to UA levels of an excited state of calcium denoted by $Ca^*(3s3p^64s^23d)$. That is, the unoccupied $1s$ level, lying below the $3s$ level of $Ar(3p^6)$ and obeying the noncrossing rule, would go to the partially occupied $3s$ level of $Ca^*(3s3p^64s^23d)$. On the other hand, in the case of strong splitting, the SA levels correlate to UA levels of $Ca^*(3s^23p^54s^23d)$. That is, the unoccupied $1s$ level, lying above the $3s$ level of $Ar(3p^6)$, would go to the partially occupied $3p$ level of $Ca^*(3s^23p^54s^23d)$. The calculations we reported in Sec. II confirm that of the two estimated possibilities this latter situation is the case. In Fig. 4(a) we display the MO correlation diagram of the occupied MO's for this latter case, where the two spin components of the $\sigma 3s$ orbital branch, one approaching the UA $3s$ level and the other the UA $3p$ level, in the way required by the noncrossing rule and shown in Fig. 3 for our calculated spin-polarized results.

As Fig. 4(a) shows, the MO's are designated at the right- and left-hand sides according to their large-R and small-R behavior, respectively, and are labeled by their appropriate SA and UA atomic-orbital limits. The convention we use for these schematic MO correlation diagrams is to designate by a single line the levels of both spin components (α and β) of an orbital, except for situations where one spin component is occupied and the other unoccupied [such as $\sigma 1s(\alpha)$], or where the noncrossing rule requires that the two occupied spin components of a given orbital correlate each to a different UA or SA atomic orbital [such as occurs for the $\sigma 3s(\alpha,\beta)$ levels].

We emphasize that the $1s2s$ state of excited helium really provides an extreme example of the effects of spin-splitting, because only two electrons are involved. Our discussion of $He^*(1s2s)+Ar(3p^6)$ indicates that we could reasonably limit ourselves to only two possibilities. With the additional effort of performing spin-polarized calculations of the $1s2s$ excited states of helium we then could resolve which of the two cases was applicable. Certainly calculations on SA and UA excited atoms lend themselves to a more definite estimation of MO correlation diagrams, but require a higher level of effort and would be helpful only for certain borderline cases.

We continue now with our example of $He^*(1s2s)+Ar(3p^6)$ to determine which of the various possible Auger processes result in MO's for the molecular ion that correlate according to guidelines (a) and (b) to the correct SA atomic-orbital levels of the product channel. In the notation of Sec. III, ϕ_1 will designate the $\sigma 2s$ orbital (or $\pi 2p$ orbital which shares the same UA $3d$ orbital limit) and ϕ_1' the continuum state of the emitted electron. ϕ_2 can then possibly be $\sigma 3p$ or $\pi 3p$, which correlate, respectively, to UA $4s$ and $3p$ atomic orbitals, as shown in Fig. 4(a). Therefore if an electron in $\sigma 3p$ participates in the Auger process the resulting UA atomic ion from which the MO's separate in the product channel would be $Ca^+(3p^64s)$. A correlation diagram for $He+Ar^+$, where $Ca^+(3p^64s)$ is the UA ion, is not shown, but one may consult instead the correlation diagram for $He+Kr^+$ in Fig. 5(b), which will be discussed shortly and which shows for the He^*+Kr case the exactly analogous situation where, in place of $Ca^+(3p^64s)$, $Sr^+(4p^65s)$ is the UA ion. Referring now to the right-hand side of Fig. 4(b), the occupied SA levels of ground-state $Ar^+(3p^5)$ all lie below the doubly occupied $1s$ level of $He(1s^2)$. This has been confirmed by spin-polarized calculations on $Ar^+(3p^5, {}^2P)$. Therefore the level of the empty $4s$ spin component of UA $Ca^+(3p^64s)$, which is split above its occupied counterpart, could not correlate in the SA limit to the partially occupied $3p$ level of $Ar^+(3p^5)$ without violating the noncrossing rule with a spin compo-

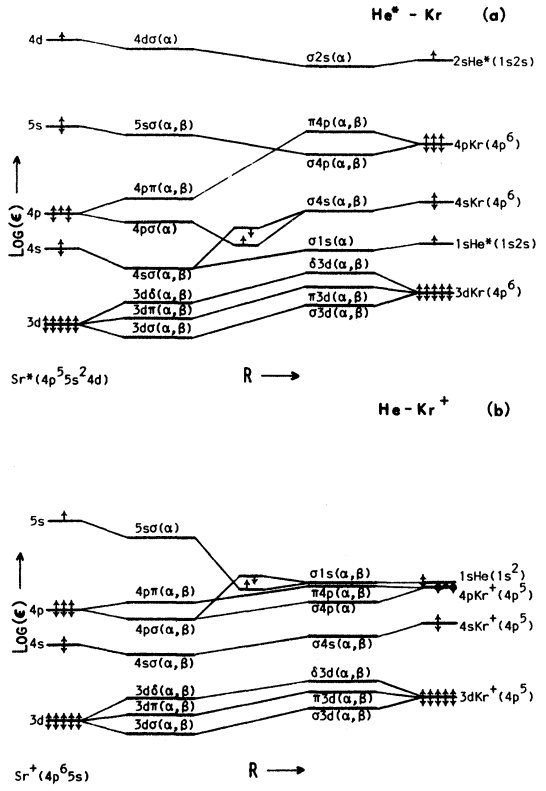

FIG. 5. Estimated MO correlation diagrams for (a) He*(1s2s)+Kr(4p⁶) and (b) He(1s²)+Kr⁺(4p⁵).

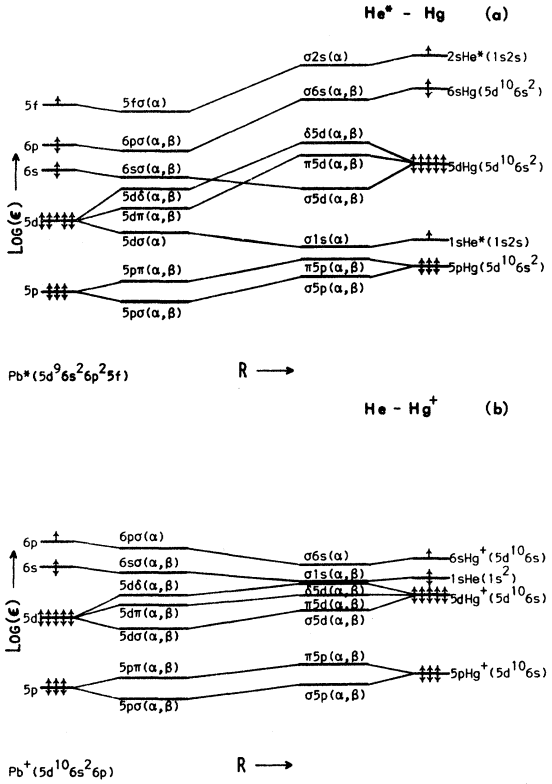

FIG. 6. Estimated MO correlation diagrams for (a) He*(1s2s)+Hg(6s²) and (b) He(1s²)+Hg⁺(6s).

nent of the σ orbital which separates to the 1s level of He(1s^2). Thus guidelines (a) and (b) do not favor an Auger process where ϕ_2 is the $\sigma 3p$ orbital. On the other hand, if ϕ_2 is the $\pi 3p$ orbital, then upon ionization the appropriate UA ion will be $[Ca^+]^*(3p^5 4s^2)$, which is shown in Fig. 4(b), and from which the MO's do correlate to the atomic levels of He(1s^2) and $Ar^+(3p^5)$ without violating guidelines (a) and (b). We therefore perform the analysis of the angular momentum contributions to the emitted electron on the basis of both Auger-type processes, aware, however, that guidelines (a) and (b) favor the one involving the $\pi 3p$ orbital.

This detailed discussion of the He*(1s2s)+Ar(3p^6) case demonstrates just how we go about analyzing PI and AI processes in terms of estimated MO correlation diagrams. In Figs. 5–7 we show the results of similar analyses performed, respectively, on He*(1s2s)+Kr(4p^6), +Hg(6s^2), and Ne*(2$p^5$3s)+Ar(3p^6).

We point out the similarity between the results for excited helium-krypton of Fig. 5(a), and those for excited helium-argon of Fig. 4(a). The MO's from the 4s and 4p levels of Kr(4p^6) have nearly exact counterparts in those from the 3s and 3p levels of Ar(3p^6). Thus we expect the unoccupied 1s level of He*(1s2s) to lie above the 4s level of Kr. A comparison of Figs. 5(a) and 4(a) suggests that He*(1s2s) in collision with Kr(4p^6) goes through the same Auger-type processes as it does in collision with Ar(3p^6). However, in Fig. 5(b) we see that the SA 4p level of $Kr^+(4p^5)$ lies very close to the 1s level of He(1s^2), enough so that the splitting of the spin components of the 4p Kr^+ level could likely result in the level of the partially occupied component lying above the 1s He level. If it lies above, then the Auger-type process favored for Kr would be different from that for Ar, and would permit the MO correlation diagram for He+Kr^+ shown in Fig. 5(b); if it lies below, then the Auger-type process favored for Kr would correspond to the one we found favored for Ar, and would permit an MO correlation diagram for He+Kr^+ analogous to the one shown for He+Ar^+ in Fig. 4(b). Considering its borderline nature, we shall analyze angular momentum contributions to the emitted electron in both these cases for He*(1s2s)+Kr(4p^6).

The MO correlation diagram for He*(1s2s)+Hg(6s^2) shown in Fig. 6(a) is the one which applies if the levels of the unoccupied 1s spin component of He*(1s2s) lies below the 5d level of ground-state

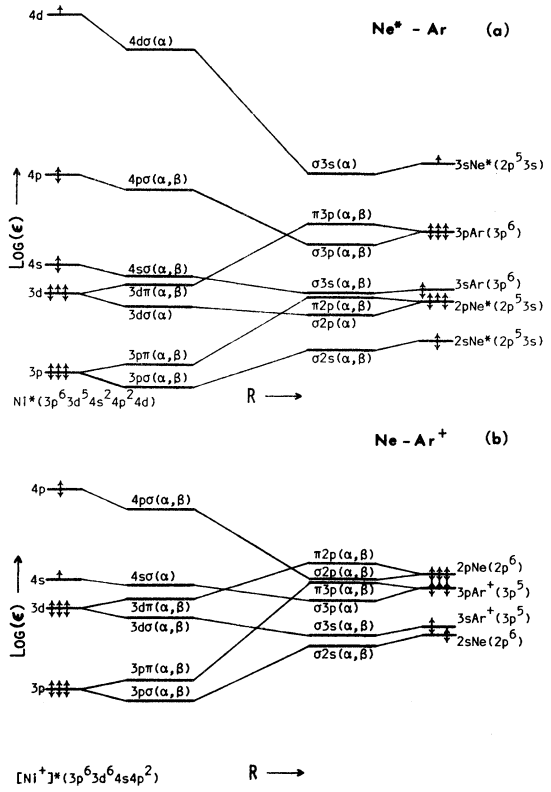

FIG. 7. Estimated MO correlation diagrams for (a) $Ne^*(2p^5 3s) + Ar(3p^6)$ and (b) $Ne(2p^6) + Ar^+(3p^5)$.

Hg. Auger processes involving $\delta 5d$, $\pi 5d$, or $\sigma 5d$ MO's can be ruled out, and Fig. 6(b) shows the MO correlation diagram for the molecular ion for an Auger process involving the $\sigma 6s$ Hg MO, in terms of which we analyze the angular momentum components of the emitted electron.

Only σ and π orbitals are occupied in the SA limit of Ne*+Ar, as seen in Fig. 7(a). This means no more than six electrons can correlate to the $3d$ orbital of the UA excited state of Ni. As a result, a very highly excited state of Ni results at the UA limit. Shown in Fig. 7(a) is the case of the $\pi 2p$ Ne* MO filled and the $\sigma 2p$ Ne* MO partially filled, corresponding to a $^{1,3}\Sigma$ molecular state. Also to be considered is the case of the $\pi 2p$ MO partially occupied and the $\sigma 2p$ MO filled, corresponding to a $^{1,3}\Pi$ molecular state and resulting in an excited state of UA Ni denoted by $Ni^*(3p^5 3d^6 4s^2 4p^2 4d)$. Auger processes involving $\sigma 3p$ and $\pi 3p$ MO's can be ruled out, whereas those involving the $\sigma 3s$ MO are allowed, resulting in the MO correlation diagram for the molecular ion shown in Fig. 7(b). This analysis assumes that the levels of both spin components of the $2p$ orbital of $Ne^*(2p^5 3s)$ lie below the $3s$ level of ground-state Ar, which, according to Fig. 7(a), is not unreasonable.

TABLE I. Minimal set of angular momentum components in the BF frame predicted for electrons emitted in PI and AI collisions.

Collision pairs	Predicted l values
He*+Ar	0, 2, 4 (favored) 1, 3
He*+Kr	0, 2, 4 1, 3
He*+Hg	0, 2, 4, 6
Ne*+Ar	0, 1, 2, 3, 4

On the basis of the MO correlation diagrams we have presented in Figs. 4–7, together with the analysis of Sec. III, we evaluate the minimal set of angular momentum contributions needed in describing the emitted electrons. These results for the various PI and AI processes are shown in Table I. The l values for He*+Ar and He*+Kr are tabulated according to which of the two previously discussed cases they belong. The favored case for He*+Ar, which is supported by our spin-polarized atomic calculations, is indicated. Because of the borderline nature of the He*+Kr estimates, both cases should be equally considered within our analysis.

A feature common to all of the collision pairs studied is that relatively few angular momentum components are predicted as being necessary to reliably represent the angular behavior of the emitted electrons in the BF frame. This result lends additional support to existing evidence that few partial waves need be kept when calculating electron angular distributions, which confirms experimental measurements.[15,20] As can be seen, He*+Hg involves only even values of l, indicating an angular distribution of emitted electrons symmetric about 90° in the BF frame. It should be pointed out that in all cases the l-value analyses in terms of the direct and exchange matrix elements of Eq. (10) give identical results, so that both couplings must be equally considered in MO descriptions.

V. DISCUSSION

The importance of MO correlation diagrams in understanding atomic collision phenomena has primarily been associated with electron promotion mechanisms in energetic atom-atom collisions.[35] In this work, however, we have studied their usefulness in connection with low (thermal) energy chemi-ionization processes.

The present approach to ionizing collisions of electronically excited atoms, based on MO corre-

lation diagrams, may readily be applied to a variety of collision partners. The number of possible ionization mechanisms may be reduced by following the two guidelines of Sec. IV for constructing MO's, and by assuming an Auger-type process. The few acceptable mechanisms that emerge from these guidelines may be enumerated and considered one by one.

The required input data are atomic energy levels of ions and neutrals in reactant and product channels at both separated- and united-atoms limits, which may be obtained from experimental tables or computationally.

Our analysis has led to two conclusions. First, it is important to use spin-polarized MO's to obtain detailed behavior at pseudocrossings. This has become clear from our MS $X\alpha$ results, which show how spin-polarized MO's for opposite spins unpair and then re-pair as one decreases the internuclear distance R. Secondly, Born-Oppenheimer rotational coupling terms, which mix molecular states of different Λ, must be considered in order to obtain all the acceptable partial waves of emitted electrons. This is particularly important, because of the R^{-2} dependence of those couplings, when one deals with MO's that converge to the same united-atoms limit.

We have chosen here to construct correlation diagrams from non-spin-polarized atomic orbitals. A better and yet practical procedure would make use of spin-polarized atomic orbitals at separated- and united-atoms limits. These, however, would have to be calculated to begin with. Comparing the present work with our previous one,[20] we have in both cases made use of adiabatic MO's obtainable in principle from separate self-consistent-field calculations for reactants and products, and of transition probabilities from diabatic couplings due to Coulomb and Born-Oppenheimer terms in the many-electron Hamiltonian.[36] The Auger mechanism plays a more prominent role in the present work. It gives equal importance to direct and exchange Coulomb integrals, and provides an alternative to older models based on interatomic electron exchange within the valence-bond approach. With the predicted l values for emitted electrons, it is clear that we could obtain angular distributions of electrons by parametrizations, as shown in Ref. 20.

ACKNOWLEDGMENT

We thank the Northeast Regional Data Center of the State University System of Florida for financial support of the calculations.

*Supported by NSF Grant No. CHE 75-01077 A01.

[1]E. E. Muschlitz, Jr., Adv. Chem. Phys. 10, 171 (1966); Science 159, 599 (1968); Ber. Bunsenges. Phys. Chem. 77, 628 (1973).
[2]A. Niehaus, Ber. Bunsenges. Phys. Chem. 77, 632 (1973).
[3]R. S. Berry, in *Molecular Beams and Reaction Kinetics*, edited by Ch. Schlier (Academic, New York, 1970), p. 193; Rec. Chem. Prog. 31, 9 (1970).
[4]R. D. Rundel and R. F. Stebbings, in *Case Studies in Atomic Collision Physics II*, edited by E. W. McDaniel and M. R. C. McDowell (North-Holland, Amsterdam, 1972), p. 549.
[5]C. Manus, Physica 82C, 165 (1976).
[6]S. Y. Tang, A. B. Marcus, and E. E. Muschlitz, Jr., J. Chem. Phys. 56, 1347 (1972).
[7]C. H. Chen, H. Haberland, and Y. T. Lee, J. Chem. Phys. 61, 3095 (1974).
[8]A. Pesnelle, G. Watel, and C. Manus, J. Chem. Phys. 62, 3590 (1975).
[9]E. Illenberger and A. Niehaus, Z. Phys. B 20, 33 (1975).
[10]H. Haberland, C. H. Chen, and Y. T. Lee, in *Atomic Physics*, edited by S. J. Smith and G. K. Walters (Plenum, New York, 1973), Vol. 3, p. 339.
[11]H. Hotop and A. Niehaus, Z. Phys. 238, 452 (1970).
[12]V. Čermák and J. B. Ozenne, Int. J. Mass Spectrom. Ion Phys. 7, 399 (1971).
[13]H. Hotop, G. Hübler, and L. Kaufhold, Int. J. Mass Spectrom. Ion Phys. 17, 163 (1975).
[14]H. Hotop and A. Niehaus, Chem. Phys. Lett. 8, 497 (1971).
[15]T. Ebding and A. Niehaus, Z. Phys. 270, 43 (1974).
[16]H. Nakamura, J. Phys. Soc. Jpn. 26, 1473 (1969).
[17]W. H. Miller, J. Chem. Phys. 52, 3563 (1970).
[18]D. A. Micha, S. Y. Tang, and E. E. Muschlitz, Jr., Chem. Phys. Lett. 8, 587 (1971).
[19]R. E. Olson, Phys. Rev. A 6, 1031 (1972).
[20]D. A. Micha and H. Nakamura, Phys. Rev. A 11, 1988 (1975).
[21]J. C. Slater and J. H. Wood, Int. J. Quantum Chem. 4, 3 (1971); J. C. Slater, Adv. Quantum Chem. 6, 1 (1972).
[22]K. H. Johnson, J. Chem. Phys. 45, 3085 (1966); Adv. Quantum Chem. 7, 143 (1973).
[23]J. C. Bellum and D. A. Micha, Int. J. Quantum Chem. Symp. 8, 229 (1974).
[24]F. Herman and S. Skillman, *Atomic Structure Calculations* (Prentice-Hall, Englewood Cliffs, N. J., 1963).
[25]D. A. Micha, Phys. Rev. A 1, 755 (1970).
[26]See for example A. Messiah, *Quantum Mechanics* (Wiley, New York, 1966), Vol. II, Appendix C, p. 1056.
[27]F. T. Smith, Phys. Rev. 179, 111 (1969).
[28]V. Sidis, in *The Physics of Electronic and Atomic Collisions, Invited Lectures, Review Papers, and Progress Reports of the Ninth International Conference on the Physics of Electronic and Atomic Collisions*, edited by J. S. Risley and R. Geballe (Univ. of Washington Press, Seattle, 1976), p. 295.
[29]C. F. Fischer, At. Data Nucl. Data Tables 12, 87 (1973).
[30]J. P. Declaux, At. Data Nucl. Data Tables 12, 311 (1973).
[31]J. B. Mann, Los Alamos Scientific Laboratory Reports LA-3690, 1967, and LA-3691, 1968 (unpublished).

[32]E. Clementi and C. Roetti, At. Data Nucl. Data Tables 14, 177 (1974).
[33]See, for example, *Handbook of Chemistry and Physics*, 48th ed., edited by R. C. Weast (Chemical Rubber, Cleveland, 1967), p. E-69.
[34]J. C. Slater, *Quantum Theory of Atomic Structure* (McGraw-Hill, New York, 1960), Vol. I, Chap. 15, p. 368.
[35]U. Fano and W. Lichten, Phys. Rev. Lett. 14, 627 (1965); M. Barat and W. Lichten, Phys. Rev. A 6, 211 (1972).
[36]Notice that the 1*s* He level in Fig. 1(a) of Ref. 20 should have been drawn as the lowest one. This does not affect any conclusions of that work.